NUCL SCI TECH (2017) 28:83
DOI 10.1007/s41365-017-0230-y

The front-end electronics design of dose monitors for beam delivery system of Shanghai Advanced Proton Therapy Facility

Bin-Qing Zhao[1,2] · Ming-Hua Zhao[1] · Ming Liu[1] · Chong-Xian Yin[1] · Hang Shu[1]

Received: 30 May 2016 / Revised: 9 January 2017 / Accepted: 19 January 2017 / Published online: 6 May 2017

Abstract A front-end electronics of dose monitor has been developed for measuring irradiation dose to the patient in Shanghai Advanced Proton Therapy Facility. The parallel plate ionization chamber is used for the dose monitoring. Unlike the traditional method of recycling capacitor integration and voltage-to-frequency conversion, this dose monitor electronics uses the trans-impedance amplifier and analog-to-digital conversion method. It performs satisfactorily, with the integral nonlinearity of less than ±0.04 nA in the range of −400 to 50 nA and the resolution of about ±0.6 nA.

Keywords Front-end electronics · Dose monitor · Proton therapy

1 Introduction

Shanghai Advanced Proton Therapy Facility (SAPT), a multi-room proton therapy system consisting of a 7-MeV Linac, a 70- to 235-MeV synchrotron and a beam switchyard, is to be installed at Shanghai Ruijin Hospital. The main advantage of proton therapy is that the charged particles deposit most of their energy over a narrow and deterministic range [1], hence the correct amount of dose delivery at correct position. So, the dose monitor should be of satisfied precision and latency [2–4].

The parallel plate ionization chamber (PPIC) is implemented for the dose monitor [5, 6]. If the energy spectrum of delivered proton is not changed, the irradiation dose can be related to the PPIC output charge from the readout electronics, which is very common in nuclear electronics design.

However, instead of a data acquisition system in nuclear physics experiment, the dose monitor controls the dose delivered by the accelerator and is similar to a sensor of a feedback system. So, the requirements of dose monitor electronics include not only the resolution and precision, but also the latency and data output rate.

The diagram of global dose control system is shown in Fig. 1. The measured dose is sent to treatment control system (TCS) by the dose monitor electronics, and TCS system switches beam on/off by turning RF-knockout (RFKO) controller on/off through the accelerator timing system. To improve the resolution, the dose monitor electronics shall be better in noise rejection, so the bandwidth shall be as narrow as possible. To improve the latency, the bandwidth and sampling rate shall be as fast as possible. Therefore, the dose monitor electronics design shall realize the balance of these paradox requirements.

For a radiation therapy system, a common way to design its dose monitor electronics is the method of recycling integration + voltage-to-frequency (V/F) converter + counter, which is adopted by the heavy ion therapy project at GSI [7] and the Heavy Ion Medical Accelerator in Chiba [8]. This method guarantees the measurement precision. However, the recycling integration causes unavoidable dead time, which is described in the Gantry1 proton therapy project at Paul Scherrer Institute (PSI) [5] and the Heavy Ion Research

✉ Bin-Qing Zhao
zhaobinqing@sinap.ac.cn

1 Shanghai Institute of Applied Physics, Chinese Academy of Sciences, Shanghai 201800, China

2 University of Chinese Academy of Sciences, Beijing 100049, China

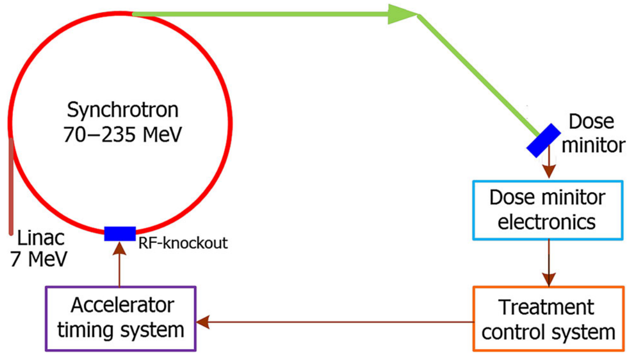

Fig. 1 Schematic diagram of the global dose control system. (Color figure online)

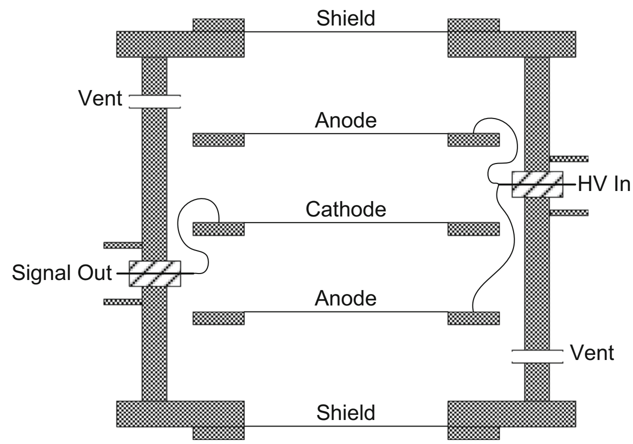

Fig. 2 Schematic diagram of the dose monitor

Facility of Lanzhou [9]. The dead time affects the accuracy of dose delivery in feedback system. In addition, *V*/*F* conversion cannot satisfy sampling rate and resolution simultaneously.

In this paper, a new approach, current-to-voltage (*I*/*V*) + analog-to-voltage converter (ADC) method is introduced for designing the dose monitor electronics. Due to the direct *I*/*V* conversion, output current of the dose monitors can be sampled by ADC and then accumulated to charge in digital domain. This method has no dead time and is of much lower latency than the recycling current integration + *V*/*F* method. Nevertheless, the bandwidth of *I*/*V* and digitalization may introduce some quantization error. Therefore, in this paper, the parameters of *I*/*V* and sampling rate are carefully chosen to comprise the balance of precision and latency, according to the proton beam current.

2 Charge and dose measurement

The dose monitors of beam delivery system are designed to measure irradiation dose to a patient's body. Two dose monitors, a main dose monitor and a sub-dose monitor, are used in the gantry nozzle. The main dose monitor is used to measure the irradiation dose and control the irradiation duration, and the sub-dose monitor is utilized to verify the irradiation dose and trigger the interlock device when the irradiation dose exceeds the defined threshold. Both monitors are PPIC vented by air, as shown schematically in Fig. 2. A bias of −2500 V is applied between the anode and cathode, which are gapped at 5 mm.

The spot scanning, which was started at the PSI [10] and GSI [11], is implemented in beam delivery system in SAPT. The proton beams are the pristine energy, changed by the synchrotron. After several energy layers, the deposited proton energy accumulates into spread-out Bragg peak (SOBP), as shown in Fig. 3. And the deposit energy or dose of SOBP can be calculated by the certain particle number with certain proton energy.

Because the proton beam of pristine energy passes through the dose monitor, the dose monitor output is proportion to the proton particle number, with different coefficients of the charge and particle number for proton beams of different energies. Through the proton therapy dosimetry workflow, these coefficients can be measured, and the relationship between dose monitor output charge and irradiation dose can be established.

3 Requirements for the front-end electronics

At the present, synchrotrons in proton therapy utilize a slow-extraction mechanism for beam extraction [12]. The beam intensity varies in time mainly due to the current ripple in the synchrotron magnets. The RFKO [13–15] slow-extraction method is implemented in SAPT, based on its quick response to start/stop signal of beam supply. The RFKO method is also useful in the spot scanning, because the beam supply can be easily started or stopped in the extraction period. However, the time structure of an extracted beam (spill) by the RFKO method has a huge ripple. Therefore, the separate function method composed of the dual frequency method (FM) and the mono-frequency RF is applied in SAPT [13], which can suppress the spill ripple sufficiently during beam extraction. Figure 4 shows the simulation results based on the FM and RF methods, with 100 µs of the accumulated period for one sampling point. The maximum irradiation time for a spot is 10 ms in our design. The calculated negative current from the dose monitor ranges from 60 to about 400 nA according to the proton beam current and the PPIC parameters. There exits some spikes in extraction spill during RFKO switching from off to on (Fig. 4). Then, the

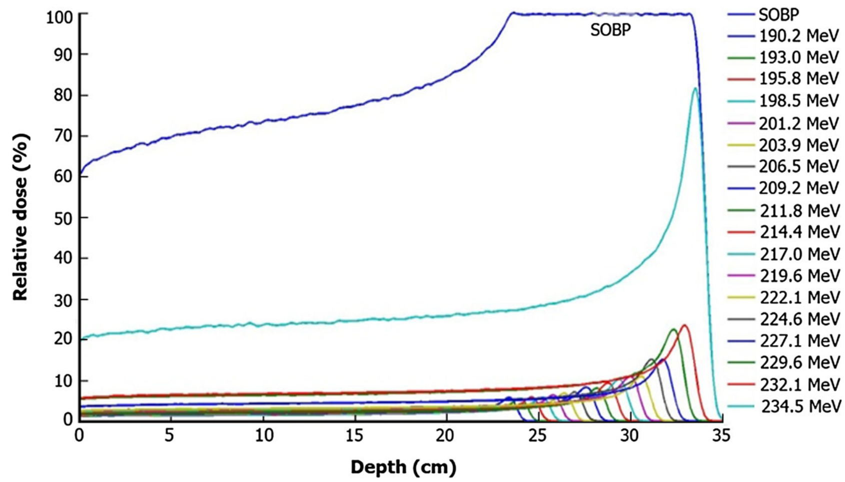

Fig. 3 Percentage depth doses distribution for high-energy (190.2–234.5 meV) proton beams and its SOBP. (Color figure online)

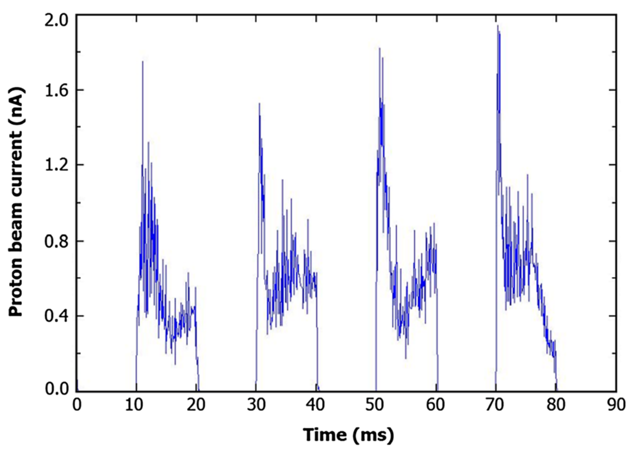

Fig. 4 Simulation of the extraction spill. (Color figure online)

current of the dose monitor electronics is set at −2500 and 0 nA so that the measured spill can be limited.

The protons are extracted by the RFKO method from the synchrotron to reach the planned number of monitor units (MUs) for each spot being scanned, and the RFKO is turned off after the dose monitor counter achieves the preset number of MUs. The accumulated charge for the spot is $Q = Ne$, where N is the number of protons and e is the electron charge. And the time integral of PPIC current is proportion to Q for the specified proton energy. As we know, the limited bandwidth of using the trans-amplifier to convert the PPIC current to voltage may loss and distorts the analog signal. Also, the analog-to-digital converter may cause absolute quantization error in measuring the variable current. A higher amplifier bandwidth means higher measuring accuracy but lower resolution due to the noise. To determine suitable bandwidth of amplifier, different spills of many spots have been simulated. Figure 5a shows the extracted protons over time for two spot sat sampling frequency of 100 kHz, using finite impulse response (FIR) low-pass filters to find the amplifier bandwidth and ensure the charge error being within a certain range after current-to-voltage conversion. Figure 5b, c shows the filtered data at 1 and 4 kHz of the pass band frequency relative to the raw data in Fig. 5a. The maximum error for total protons in one spot is less than 0.016 and 0.0159%.

The dosimetry error should be less than ±3% to satisfy medical requirement. And the relative accuracy of the delivered dose should be better than ±2% of the specified dose. The remaining 1% is assigned to the dose monitor electronics. From Fig. 5, 1 kHz of the amplifier bandwidth is feasible to reach the defined charge error of ±1%. The resolution of the dose monitor is defined in a range of ±1%, or ±0.6 nA. In addition, the linearity is chosen to be within ±0.2%, or ±0.12 nA.

The response of the dose monitor electronics must be fast enough to satisfy the latency of beam delivery system, <0.4 ms. The transition duration to stop spill by switching off RFKO is about 0.3 ms, and the ion collection time in dose monitor is about 70 μs. The latency of dose monitor electronic should be less than 30 μs, including acquisition time, signal transfer time and treatment control system latency. Finally, the latency of dose monitor electronics decreased to 20 μs. Specifications of the dose monitor electronics are: range, −2500 to 0 nA; analog bandwidth, 1 kHz; linearity, ±0.2%; resolution (2σ), ±1%; and latency, 20 μs.

4 Electronics design

In order to satisfy the latency requirement, the sampling rate of ADC is set at 100 kHz, and the latency time of ADC is only one sampling period. The accumulated charge can be calculated by:

$$Q = \Delta T \sum_{n} V(n)/G, \tag{1}$$

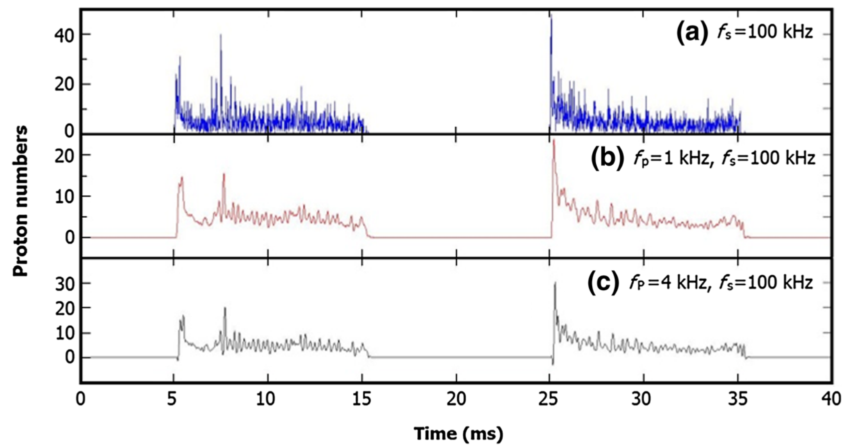

Fig. 5 The extracted protons over time for two spots (**a**). **b**, **c** The data after FIR filter at different passband frequencies. (Color figure online)

where ΔT is the sampling interval, $V(n)$ is the corresponding voltage and G is amplifier gain. To achieve a higher accuracy, the bandwidth of *I*/*V* must be larger than 1 kHz to match the analog signal bandwidth. In this design, *I*/*V* converter is a key component in the dose monitor electronics. It should achieve the bandwidth and suppress the noise to reach the resolution of dose monitors. Moreover, the output voltage should also be matched to the analog input range of ADC.

Considering the balance between common-mode noise suppression and amplifier noise reduction, the amplifier circuit is based on a two-stage cascaded structure. Also, it is convenient to adjust the gain and bandwidth of each module. The two stages are based on the trans-impedance amplifier (TIA) and the low-noise amplifier (LNA), respectively. Figure 6 shows the circuit. The trans-impedance gain R_1 is 249 kΩ, and the resistor R_3 is 249 Ω and R_4 is 1 kΩ, so a total gain of 10^{-6} can be reached to cover an output voltage range of 0–2.5 V theoretically.

Selection of capacitors C_2 and C_4 shall match the analog current bandwidth, and the bandwidth of the second amplifier shall be larger than the first one to reduce loss of useful signal. On the other hand, they are correlated with common-mode noise suppression and amplifier noise reduction. The main problem of this part is how to balance between the amplifier bandwidth and the common-mode

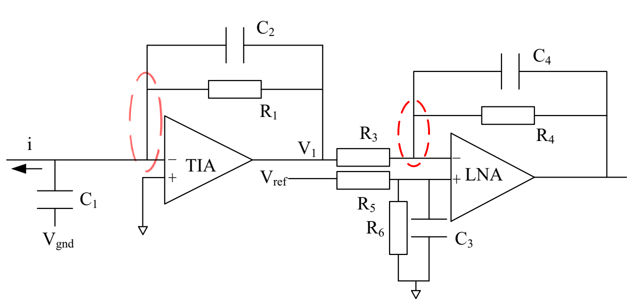

Fig. 6 Simplified schematics of the two-stage cascaded circuit. (Color figure online)

noise suppression. The common-mode noise caused by the grounding lines is given as

$$V_{cm}(s) = V_{gnd}(sR_1C_1)/(1 + sR_1C_2), \tag{2}$$

where C_1 and C_2 are defined as the capacitance of dose monitors and the first amplifier, R_1 is the feedback resistance of the first module and V_{gnd} is the ground noise. However, the output voltage $V_1 = iR_1/(1 + sR_1C_2)$; then, C_2 should be small enough to increase bandwidth of the amplifier. From Eq. (2), C_2 should be large to reduce common-mode noise, improve SNR (signal–noise ratio) and increase the bandwidth of analog signal. So, in our design, $C_2 = 560$ pF. In addition, the noise of amplifier depends largely on the voltage noise and resistor thermal noise, while the ratio between them is around 4 based on the second-stage gain. Therefore, we need to care more about the voltage noise of electronics:

$$V_N(s) = V_{N_2}\frac{5 + sR_4C_4}{1 + sR_4C_4} + 4V_{N_1}\frac{1 + sR_1(C_1 + C_2)}{(1 + sR_1C_2)(1 + sR_4C_4)}, \tag{3}$$

where C_4 is the second amplifier, R_4 is the feedback resistance and V_{N_1} and V_{N_2} are the input voltage noise of each amplifier, respectively. So, we shall select proper value of C_2 and C_4 to improve SNR. Then, $C_4 = 100$ nF in our final design.

Considering the output voltage caused by the offset voltage and the bias current at zero input current, V_{ref} is introduced to provide a reference voltage so that the input voltage of ADC can be 0–2.5 V. The ratio $b = R_5/R_6$ is based on Eq. (4).

$$\frac{1 + a}{1 + b}V_{ref} + V_{osl} < V_{ref}, \tag{4}$$

where $\alpha = R_4/R_3$ and V_{osl} is output offset voltage in the case of no current.

Finally, the output voltage can be described using the following equation under direct current (DC) mode:

$$V(i) = 2.3147 + 10^{-3} \cdot i + \Delta V \quad (5)$$

where i is the input current in nA and ΔV depends on the input bias current, offset voltage of the circuit and the leakage current. A 2.5-V full-scale, 16-bit ADC is employed as a key digital component with sampling rate up to 100 kHz to ensure fast conversion rate and high performance.

According to electromagnetic compatibility requirements of medical electrical equipment in YY0505-2012 [16], there are some tips in the printed circuit board (PCB) design. Figure 6 shows the guard rings to enclose the op amp inputs and reduce leakage current, as noted by the red dotted line. The input current signal is injected by shielded cables in the middle layer, but near a ground plane. All analog signals are guarded via a metal box to shield electromagnetic radiation. Furthermore, the digital circuit in a different power supply should be isolated from other parts to broadcast electromagnetic waves.

5 Results and discussion

For most of the tests, the KEITHLEY current source 6220 [17] was used to generate a precise current. The current generator provided a current range of 0–2500 nA, with an accuracy of 0.1%. The ISEG SHQ224M [18] was used to power the dose monitors. Its maximum dual output voltage is 4 kV with ripple of <0.5 mV pp. Performance of this front-end electronics, with the powered dose monitors, is mainly determined by linearity of current-to-voltage conversion, resolution and background noise.

5.1 Linearity of current-to-voltage conversion

Nonlinearity of this electronics system is measured by inputting −2400 to 0 nA in 100-nA steps. Figure 7a demonstrates good linearity between the measured voltage and the input current, with a slope of $y = 2.3721 + 10^{-3}x$ ($2.3721 + 0.001x$). So the total gain (output over input) is 0.001 V/nA, which is equal to the amplifier gain. As shown in Fig. 7b, the maximum integral nonlinearity (INL) is less than ± 0.04 nA cover a current range from −400 to −50nA, which is much lower than the requirements of ±0.12 nA. These verify that the nonlinearity of front-end electronics can be well designed by the two-stage cascade circuit, as discussed before. In order to attain an accuracy request of dose measurement with intensity modulated conformal proton therapy (IMPT), one count is defined as 0.2 pC in this design.

5.2 Resolution

The resolution of charge measurement, which depends largely on the current resolution of the electronics system, is an important indicator to evaluate the performance. It is clear that the charge is equal to the integral of current times to times and the integration time is set to a constant value

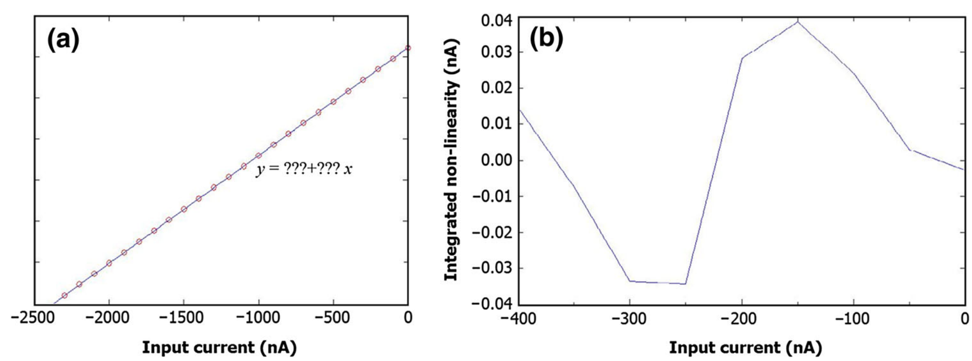

Fig. 7 Linearity (**a**) and INL (**b**) of the dose monitor electronics

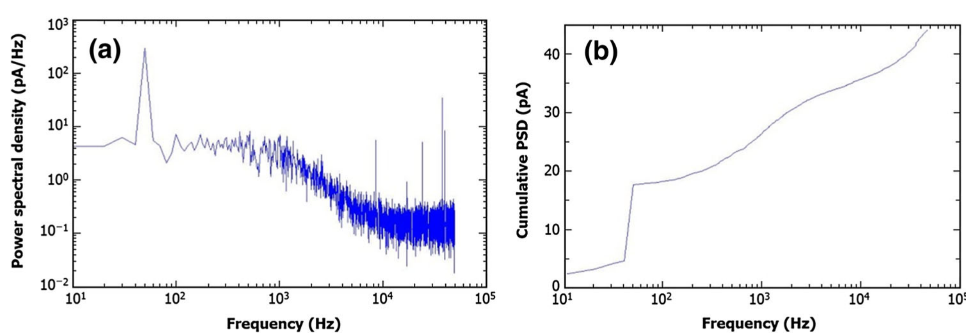

Fig. 8 PSD (**a**) and integral power spectrum (**b**) of the electronics output. (Color figure online)

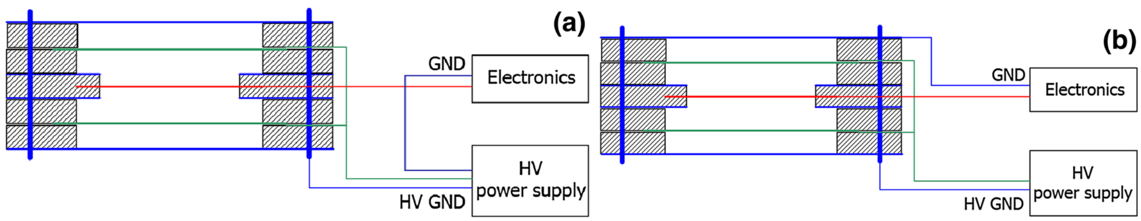

Fig. 9 Layout of the monitor grounding system. **a** The grounding lines of electronics and high-voltage power supply are connected together; **b** only one grounding point. (Color figure online)

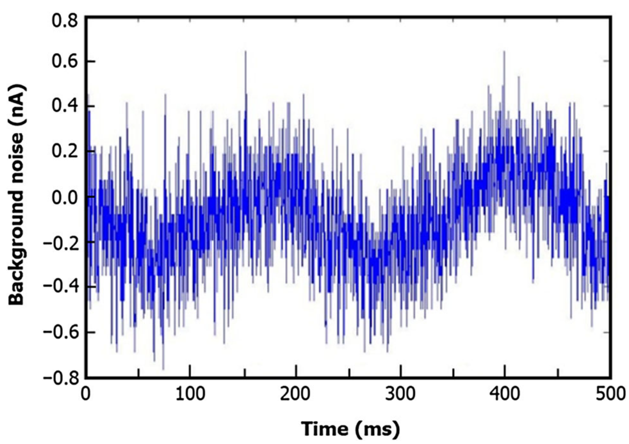

Fig. 10 Background noise with high voltage in dose monitor. (Color figure online)

in this method. Therefore, the current power density spectrum is tested over a frequency range of 10 Hz–100 kHz and then integrated. From the measured power spectral density (PSD) and the integral power spectrum (Fig. 8), the power density peak is at 50 Hz and the noises are mainly in high frequencies, but the electronics noise is less than 60 pA (r.m.s). So, we will design a least-mean-square (LMS) filter to attenuate 50 Hz power frequency interference and digital FIR low-pass filter to reduce high-frequency noises with low latency [19].

5.3 Background noise with high voltage in dose monitors

To reduce background noise, it is important to choose a good method to ground the dose monitors, the high-voltage source and the electronics system, i.e., to minimize the influence on common-mode rejection capability and electromagnetic compatibility (EMC). For this reason, the dose monitor electronics should immune the noise of high-voltage power (HV), and the weak current in dose monitors should be isolated with the interference from HV. To achieve the best performance, after many experiments, we chose the layout with only one grounding point in the whole monitor system (Fig. 9). Figure 10 shows that the background noise of the HV-biased dose monitors is improved, which completely meets the requirements of the electronics noise in the range of ±0.6nA. Compared with the peak-to-peak value of a few decades nano-ampere in the old design, this is much lower in the improved design now and verifies the correctness of the grounding mode.

6 Conclusion

The front-end electronics of dose monitors for the beam delivery system in SAPT has been developed. The linearity from −500 to 40 nA is within ±0.04 nA, and the electronics noise is less than 60 pA (r.m.s). Moreover, the background noise with high voltage is within ±0.6 nA. All the requirements have been satisfied in our design. With the techniques adopted in this paper, this front-end electronics of dose monitors can be totally used to measure the irradiation dose in the proton therapy.

References

1. D.T.L. Jones, H.D. Suit, Y. Akine et al., *Prescribing, Recording, and Reporting Proton-Beam Therapy* (Oxford University Press, ICRU R78, Oxford, 2007)
2. P.J. Bryant, L. Badano, M. Benedikt et al., Proton-Ion Medical Machine Study. CERN-2000-006 and CERNPS-2000-007(DR) (2000)
3. J. Wu, H.W. Du, S. Xue et al., Gantry optimization of the Shanghai Advanced Proton Therapy Facility. Nucl. Sci. Tech. **26**, 040201 (2015). doi:10.13538/j.1001-8042/nst.26.040201
4. H. Shu, S.-X. Fang, X.-L. Guan et al., Irradiation methods and nozzle design for the advanced proton therapy facility. Chin. Phys. C **34**, 516–520 (2010)
5. S. Lin, T. Boehringer, A. Coray et al., More than 10 years experience of beam monitoring with the Gantry 1 spot scanning proton therapy facility at PSI. Med. Phys. **36**, 5331–5340 (2009). doi:10.1118/1.3244034
6. C.P. Karger, O. Jäkel, H. Palmans et al., Dosimetry for ion beam radiotherapy. Phys. Med. Biol. **55**, 193–234 (2010). doi:10.1088/0031-9155/55/21/R01
7. H. Stelzer, Tumor therapy with heavy ions at GSI. Nucl. Phys. B (Proc. Suppl.) **61B**, 650–657 (1998). doi:10.1016/S0920-5632(97)00633-6
8. M. Torikoshi, K. Noda, E. Takada et al., Beam monitor system for high-energy beam transportation at HIMAC. Nucl. Instr.

Methods Phys. Res. A **435,** 253 (1999). doi:10.1016/S0168-9002(99)00569-0
9. Z. Xu, R. Mao, L. Duan et al., A new multi-strip ionization chamber used as online beam monitor for heavy ion therapy. Nucl. Instr. Methods Phys. Res. A **729**, 895–899 (2013). doi:10.1016/j.nima.2013.08.069
10. E. Pedroni, R. Bacher, H. Blattmann et al., The 200-MeV proton therapy project at the Paul Scherrer Institute: conceptual design and practical realization. Med. Phys. **22**, 37–53 (1995). doi:10.1118/1.597522
11. H. Eickhoff et al., Accelerator aspects of the cancer therapy project at the GSI Darmstadt, in *EPAC96 Proceedings* (1996)
12. J.Q. Zhang, M.T. Song, B.W. Wei, Design of synchrotron for hadron therapy. Chin. Phys. C **31**, 1122–1125 (2007)
13. K. Noda, T. Furukawa, S. Shibuya et al., Advanced RF-KO slow-extraction method for the reduction of spill ripple. Nucl. Instr. Methods Phys. Res. A **492**, 253–263 (2002). doi:10.1016/S0168-9002(02)01319-0
14. T. Furukawa, K. Noda, Fast beam cut-off method in RF-knockout extraction for spot-scanning. Nucl. Instr. Methods Phys. Res. A **489**, 59–67 (2002). doi:10.1016/S0168-9002(02)00895-1
15. D. Shi, L. Ouyang, M. Gu, The RF-knockout slow-extraction for Shanghai proton therapy facility. Nucl. Tech. **35**, 231–235 (2012). **(in Chinese)**
16. J Liu et al., Medical electrical equipment-Part 1–2: General requirements for safety-Collated standard: Electromagnetic compatibility-requirements and tses (CFDA, 2012), p. 20–28, YY 0505–2012
17. Information about this product can be found at Tektronix web page: http://www.tek.com/keithley
18. Information about this product can be found at Iseg web page: http://iseg-hv.com/en/
19. B.Q. Zhao, C.X. Yin, M. Liu et al., Design of digital filter based on dose monitor. Nucl. Electron. Detect. Tech. **36**, 26–29 (2016). **(in Chinese)**